Pronounced shape change induced by quasiparticle alignment

A. Algora,[1,2] G. de Angelis,[1] F. Brandolini,[3] R. Wyss,[4] A. Gadea,[5] E. Farnea,[5] W. Gelletly,[6] S. Lunardi,[3] D. Bazzacco,[3] C. Fahlander,[1,7] A. Aprahamian,[8] F. Becker,[9] P. G. Bizzeti,[10] A. Bizzeti-Sona,[10] D. de Acuña,[1] M. De Poli,[1] J. Eberth,[9] D. Foltescu,[1] S. M. Lenzi,[3] T. Martinez,[1] D. R. Napoli,[1] P. Pavan,[3] C. M. Petrache,[3] C. Rossi Alvarez,[3] D. Rudolph,[7] B. Rubio,[5] S. Skoda,[9] P. Spolaore,[1] R. Menegazzo,[3] H. G. Thomas,[9] and C. A. Ur[3]

[1]*Istituto Nazionale di Fisica Nucleare, Laboratori Nazionali di Legnaro, I-35020 Legnaro, Italy*
[2]*Institute of Nuclear Research of the Hungarian Academy of Sciences, Pf. 51, H-4001, Debrecen, Hungary*
[3]*Dipartimento di Fisica dell'Università, and Istituto Nazionale di Fisica Nucleare, Sezione di Padova, I-35131 Padova, Italy*
[4]*KTH-Kärnfysik, Frescativ. 24, S-104 05 Stockholm, Sweden*
[5]*Instituto de Física Corpuscular, E-46100 Valencia, Spain*
[6]*Department of Physics, University of Surrey, Guildford GU2 5XH, United Kingdom*
[7]*Department of Physics, Lund University, S-22100 Lund, Sweden*
[8]*Department of Physics, University of Notre Dame, Notre Dame, Indiana 46556*
[9]*Institut für Kernphysik, Universität zu Köln, D-50937 Köln, Germany*
[10]*Dipartimento di Fisica dell'Università, and Istituto Nazionale di Fisica Nucleare, Sezione di Firenze, I-50125 Firenze, Italy*

Mean lifetimes of high-spin states of ^{74}Kr have been determined using the Doppler-shift attenuation method. The high-spin states were studied using the ^{40}Ca(^{40}Ca, $\alpha 2p$) reaction at a beam energy of 160 MeV with the GASP γ-ray spectrometer. The ground-state band and negative parity side band show the presence of three different configurations in terms of transitional quadrupole deformations. A dramatic shape change was found along the ground-state band after the S-band crossing. The deduced quadrupole deformation changes are well reproduced by cranked Woods-Saxon Strutinsky calculations.

PACS number(s): 21.10.Re, 21.60.Cs, 21.60.Jz, 23.20.Lv

In recent years proton rich Kr isotopes have been the ground for extensive nuclear structure research. The low density of single-particle levels in this mass region of the nuclear chart gives rise to pronounced shape effects [1]. Large shell gaps at $Z,N = 34,36$ for oblate shapes and at $Z,N = 38,40$ for prolate shapes result in very deformed ground-state configurations and prolate-oblate shape coexistence [1–5]. All these features have been found experimentally in ^{74}Kr. In Refs. [6,7] evidence for large quadrupole deformation in the ground-state band was obtained from lifetime measurements, and in Ref. [8] an isomer was interpreted as a highly deformed oblate 0^+ state.

In the present work we focus our interest on the determination of lifetimes of high-spin states of ^{74}Kr using the Doppler-shift attenuation method (DSAM). The main goals are to extend the former knowledge of lifetimes [6,7] to the states above the bandcrossing in the ground-state band and to deduce the transitional quadrupole moments of the studied levels. Comparison of the new results with theoretical calculations will allow us to investigate the reinforcement of shell effects due to the coherent contribution of proton and neutron particles in identical orbits, and to study the core-polarization effects of different configurations. From this information it will also be possible to further clarify the importance of shell gaps in this region.

The high-spin states of ^{74}Kr were populated using the ^{40}Ca$+^{40}$Ca reaction at a bombarding energy of 160 MeV. The beam was delivered by the Tandem XTU accelerator at the Legnaro National Laboratory and the recoiling ions produced in the 0.9 mg/cm^2 ^{40}Ca target were stopped in a 10 mg/cm^2 gold backing. The emitted γ rays were detected using the GASP array [9], composed of 40 Compton-suppressed high-efficiency HPGe detectors and an inner BGO ball of 80 crystals. Events were collected on tape under the condition that a minimum of two Compton-suppressed Ge detectors and one BGO element from the multiplicity filter fired in coincidence. The beam intensity was around 3 pnA, giving a singles rate of ~ 10 kHz in the individual Ge detectors and an event rate of ~ 4 kHz.

For the lifetime analysis, the data were sorted into $\gamma\gamma$ matrices, each having on one axis the detectors of one of the rings at 34°, 60°, 72°, 90°, 108°, 120°, and 146°, and, on the second axis, any other detectors. For the energy and efficiency calibrations, ^{152}Eu and ^{56}Co sources were used.

In a typical DSAM lifetime analysis one of two possible procedures are followed. These procedures are called gate on a transition below (GTB), when the gate for generating the spectra is taken on a transition below the level of interest, or gate on a transition above (GTA), when the spectra is generated using a gate above the level of interest. The GTA procedure avoids the sidefeeding contribution to the lifetimes, but requires putting a gate on a broadened line to include its entire line shape. The use of a wide gate can lead to contaminated spectra. In most cases, this procedure cannot be followed due to the high statistics required. On the other hand, the first procedure (GTB), which is the one used in this work, requires a careful determination of the transition intensities, in order to reduce the number of uncertainties related to the sidefeedings.

For the line shape analysis the Monte Carlo code LINE-SHAPE [10] was used. This code incorporates a description of the nuclear stopping power according to the LSS theory [11] and MINUIT, [12] for the error analysis. For the electronic stopping power a corrected [13] Northcliffe-Schilling param-

etrization [14] was used. The LINESHAPE code is a package formed by three programs. The first one generates a large number of simulations of the possible slowing down processes of the recoil nucleus, accounting for the reaction kinematics. The second one calculates the $D(t,v)$ distribution (the projection of the recoil velocity along the direction of the detected γ ray as a function of time), and also takes into account the opening angle of the detectors. The third program performs the fit procedure of the data in an interactive way and models the level feeding with one or more cascades.

In the particular case of our analysis the slowing down process of the nucleus was reproduced using 10 000 simulations. The contribution of the sidefeeding to the lifetime of each level was modeled using a cascade of two transitions of adjustable lifetime. The sidefeeding intensities were extracted from the spectra generated at 90°; in this way the only free parameters in the fit procedure were the level lifetimes and the sidefeeding lifetimes.

The level scheme of ^{74}Kr is known from Ref. [15]. In Fig 1. we show the part of the level scheme which is relevant to our analysis. It is clear from Fig. 1 that using the GTB method, it is difficult to obtain spectra for the ground-state band (GSB) transitions which are not contaminated by the transitions of the negative parity side band (overlap between the 768, 966, and 1287 keV transitions of the ground-state band, and the 767, 954, and 1277 keV transitions of the negative parity side band) and at the same time fulfill the requirement of having high statistics. Therefore, in order to obtain precise lifetime values for the states of the GSB, it is necessary to take into account the contribution of the negative parity band transitions to the line shapes of the GSB in the deconvolution process.

We have first determined the lifetimes of the negative parity side band. The spectra for this part of the analysis were generated by putting a gate on the strongest transition connecting the two bands, i.e., the 1586 keV line. In the negative parity band we can observe all γ-ray transitions up to the $21^- \rightarrow 19^-$ 1658 keV gamma ray. Both the 1658 and the 1532 keV gamma rays show a full Doppler shift. For the following transition in the band, the 1410 keV transition, one can determine an effective lifetime of 0.05(3)ps. The lifetimes of the transitions of the negative parity band are presented in Table I. All of the lifetime values of this band can be fitted with a constant quadrupole moment of 2.8 e b. The determination of the lifetime of the 767 keV transition requires the use of spectra generated by gating on the weak 555 keV γ line, since the gate on the 1586 keV transition is not able to separate the 767 and 768 keV γ lines of the negative parity band and ground-state band, respectively.

For the analysis of the ground-state band the spectra were generated by setting gates on the 446 keV and 558 keV γ lines. The spectra created using the 558 keV gate were generally less contaminated. For that reason most of the analysis was performed using this gate. The information on lifetimes of the previously analyzed negative parity band was used to take into account the contamination due to the similarity of the energies of the transitions. The contribution of the contaminants to the line shapes of the GSB was determined using the intensity ratio obtained from the spectra at 90°.
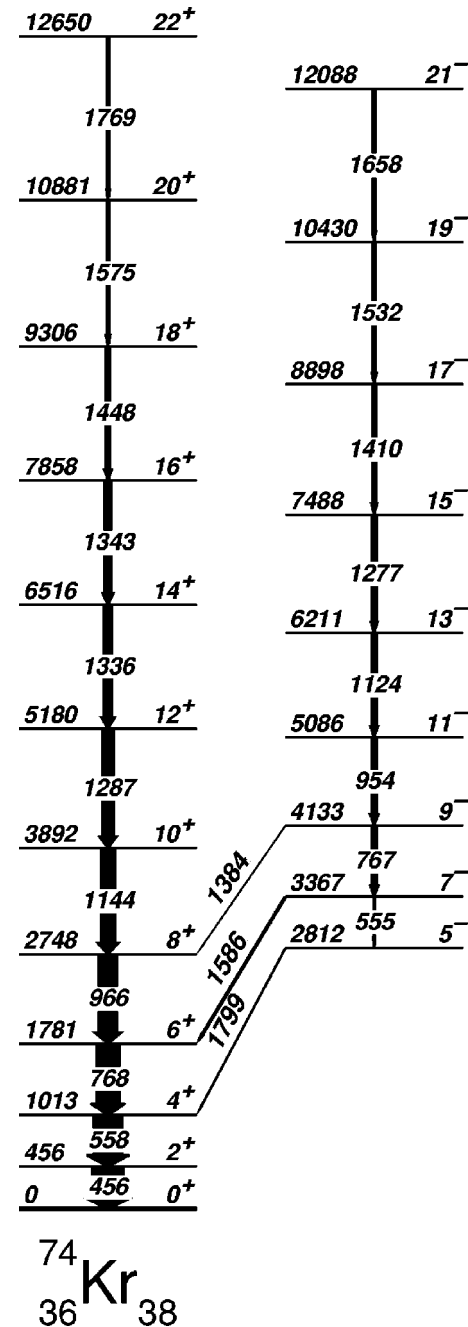

FIG. 1. Partial level scheme of ^{74}Kr relevant to this work.

The highest transition seen in the ground-state band has an energy of 1769 keV and connects the 22^+ and the 20^+ levels. As in the case of the negative parity side band, this and also the transition below in the cascade (1575 keV) show a full Doppler shift. The lifetime of the following 1448 keV transition could be determined giving a value of 0.08(3)ps. The results of our analysis are presented in Table I. The transitional quadrupole moments show a clear evolution from 3.0 e b to 2.1 e b along the ground-state band. In Fig. 2. the results of a typical fitting procedure are shown.

Deformation properties are one of the most crucial probes of nuclear structure models. The $A = 80$ mass region, where sudden changes of deformation occur, is an important testing

TABLE I. Mean lifetimes and transitions strengths for the studied bands of ^{74}Kr.

Transition	E_γ (keV)	I_γ (%)	τ(ps) Pres.	τ(ps) Prev. [6]	τ(ps) Prev. [7]	B(E2) (e^2fm$^+$)	$|Q_t|$ (e b)
$6^+ \to 4^+$	768.0	100	1.08(14)	0.90(15)	0.91(10)	2824(370)	3.0(2)
$8^+ \to 6^+$	966.5	79	0.35(5)	0.28(5)	0.24(4)	2762(400)	2.9(2)
$10^+ \to 8^+$	1144.4	63	0.16(3)	0.10(3)	0.10(3)	2596(500)	2.8(2)
$12^+ \to 10^+$	1287.2	51	0.10(2)	0.18(5)	$\leqslant 0.11$	2307(480)	2.6(2)
$14^+ \to 12^+$	1336.2	42	0.13(3)			1473(360)	2.1(2)
$16^+ \to 14^+$	1342.6	33	0.12(3)			1558(420)	2.1(2)
$18^+ \to 16^+$	1447.5	24	0.08(3)			1604(700)	2.1($^{+5}_{-3}$)
$9^- \to 7^-$	766.9	25	1.18(12)			2603(270)	2.8(1)
$11^- \to 9^-$	953.5	25	0.39(4)			2652(280)	2.8(1)
$13^- \to 11^-$	1124.2	24	0.17(3)			2671(490)	2.8(2)
$15^- \to 13^-$	1277.0	21	0.09(2)			2668(620)	2.8(2)
$17^- \to 15^-$	1410.4	18	0.05(2)			2922(1390)	2.8(2)

ground for our understanding of the low-lying collective modes. In this region the onset of deformation has been discussed in the Sr isotopes and has been related to the simultaneous occupation of $g_{7/2}$ and $g_{9/2}$ orbitals [16]. However, in the Woods-Saxon Strutinsky approach, the origin of the deformation for the light Kr isotopes has been related to the large deformed shell gaps at prolate shape ($\beta_2 = 0.35 - 0.4$) for $N = Z = 38$ and oblate shape ($\beta_2 \leqslant -0.3$) for $N = Z = 36$. Hence, one expects shape coexistence and deformation changes to occur in these nuclei. For the case of ^{74}Kr, total Routhian surface (TRS) calculations [17–19] predict prolate-oblate shape coexistence at low spins. The prolate-oblate energy difference is estimated to be 200 keV, whereas the experimental value is of about 500 keV [8]. Our data, which do not allow the determination of the lifetimes of the levels at very low excitation energy (the 456 and 558 keV transitions do not show any line shapes), reveal three different values of the transitional quadrupole moment, indicating strong polarization effects. The ground-state band beyond the perturbation at $I = 2\hbar$ (Fig. 1) is highly deformed with a Q_t value of 3 e b ($\beta_2 = 0.38$). In the calculations, we obtain a value of 3.45 e b, corresponding to $\beta_2 = 0.43$ and to a rather small $\beta_4 = 0.005$. The quadrupole moment is calculated as the expectation value of $\langle Q_{20} \rangle$ and $\langle Q_{22} \rangle$ from the wave functions at the minimum of the Routhian surface. Since the absolute value of the transitional quadrupole moment is connected with uncertainties in both experiment and theory, we focus in the following on the relative changes.

At $\hbar\omega = 0.6$ MeV, the minimum at prolate shape becomes very soft and at the next calculated frequency, only a prolate minimum at small deformation remains. Due to the simultaneous alignment of proton and neutron particles, predicted by calculations at $\hbar\omega \approx 0.65$ MeV, four particles are not contributing to the collective behavior. The pronounced effect before and after the band crossing is clearly seen in the calculations (see Figs. 3 and 4).

Two different factors contribute to the shape change at prolate deformation:

(a) The aligning particles originating from the $g_{9/2}$ unique parity subshell are expected to contribute less to the quadru-

pole moment. Since a fully aligned particle has a density distribution that is essentially oblate, one may expect a weakening of the polarizing factor of the $g_{9/2}$ quasiparticles. A similar effect has been suggested to be responsible for the reduction of the quadrupole moments at high spins in the rare earth region [20,21]. By calculating the quadrupole moment from the intrinsic wave functions at each frequency and at constant deformation, one is sensitive to the above-mentioned effect. In the frequency range considered we notice only a very slight change ($\delta Q_{20} = 0.01$ e b). This lack of feedback from the intrinsic shape to the single particle po-
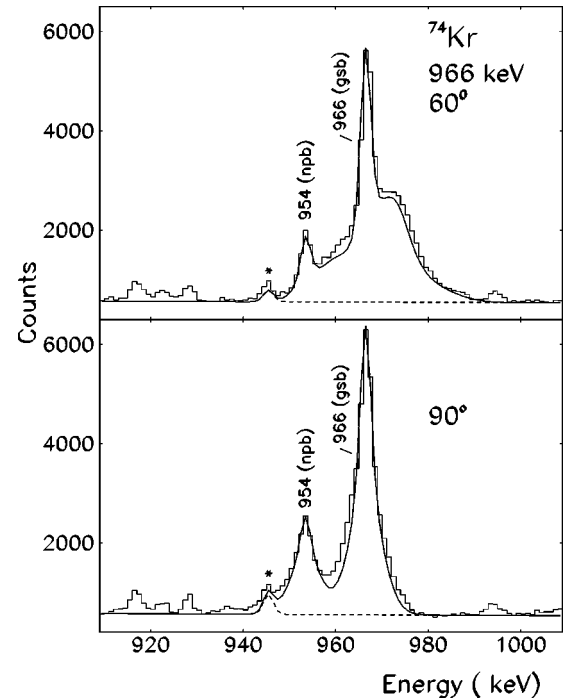

FIG. 2. Typical line shape fit in ^{74}Kr for the transition 966 keV of the ground-state band (GSB). The continuous line shows the results of the fit procedure with the contribution of the 954 keV line of the negative parity side band. The symbol ''*'' labels a contaminant peak.
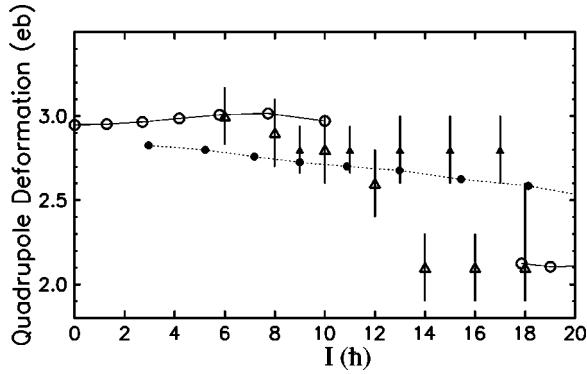
FIG. 3. Comparison of the experimentally determined quadrupole shapes (triangles) with the theoretical predictions (circles). Empty symbols correspond to the ground-state band data. Filled symbols label the data for the negative parity side band. The theoretical values are renormalized by a factor of 0.87, in order to facilitate the comparison to experiment.

FIG. 5. Model calculations to illustrate the dependence of the $g_{9/2}$ quasiproton alignment on deformation. The calculations are performed at axial shapes for 36 protons and the pairing gap is kept constant. The rotational frequency considered is ranging from $\hbar\omega = 0.0$ to $\hbar\omega = 1.3$ MeV. The alignment gain is extracted integrating the J_2 moment of inertia after the quasiparticle alignment. At spherical shape the alignment is taken directly from the calculated I_x.

tential has been discussed in Ref. [22]. The reason for this small value is related to the fact that the $g_{9/2}$ protons and neutrons are close to the Fermi-surface and are essentially of quasiparticle (QP) nature. The K mixing does not effect the total quadrupole moment very much and, even at $\hbar\omega = 1.0$ MeV, the reduction amounts only to $\delta Q_{20} = 0.15$ e b. Moreover, the shell gap at $N = 38$ is quite pronounced and is still large at that rotational frequency.

(b)A shape-driving factor related to the angular momentum gain in the alignment process. To illustrate such effect we have performed model calculations at axial deformation for different β_2 values. The angular momentum gain is extracted from the dynamical J_2 moment of inertia (for spherical shape we have used the change in the calculated I_x). Clearly the rotational alignment of a given high-j orbit has its maximum at spherical shape (Fig. 5). Since $dI/d\beta$ is negative, the nucleus can gain additional alignment by reducing the deformation.

One is dealing here with a balance between shell correction that may favor more deformed shapes, and angular momentum which is gained more efficiently at less deformed shapes. This balance has been discussed in a slightly different context for states in superdeformed Hg nuclei [23]. There

it is a subtle effect, resulting in a smooth shrinking after the neutron alignment, whereas here we deal with a rather pronounced jump in deformation due to the large $dI/d\beta$ in the band crossing region. To give an example, at $\hbar\omega = 0.6$ MeV, just below the bandcrossing, the angular momentum extracted from the TRS calculations is, at $\beta_2 = 0.39$, $I = 9.6\hbar$, and at $\beta_2 = 0.29$, $I = 7.5\hbar$. Since we are dealing with mainly collective rotation, the angular momentum is of course larger at larger deformation. In contrast, at $\hbar\omega = 0.7$ MeV, the $g_{9/2}$ protons and neutrons have aligned at the smaller deformation, giving a difference in angular momentum of $4.3\hbar$ between the two structures. One should note here that the dominant part of this difference is due to protons ($dI_p = 2.6\hbar$). Hence, by readjusting the shape, the nucleus can gain angular momentum at lower cost. The effect in the TRS calculations is larger than the one illustrated in Fig. 5 since the alignment gain saturates at considerably lower frequency at the smaller deformation. Such shape change therefore is mainly driven by the interplay between single particle alignment and collective rotation. The softness of nuclei in the $A = 80$ region induces such drastic effects.

For the negative parity band, we do not find such strong shape change (Fig. 6). Since we are dealing with a proton
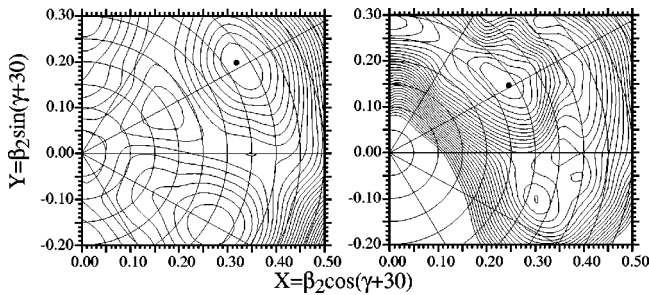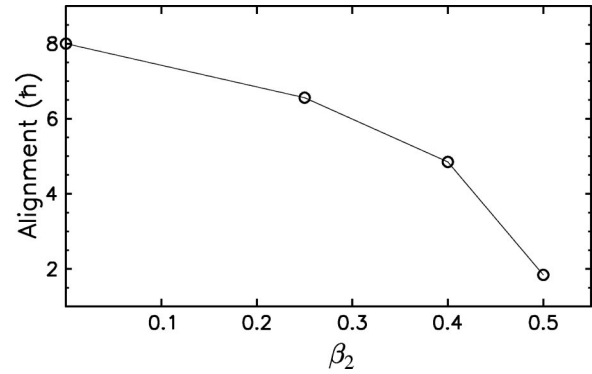

FIG. 4. The total Routhian surface calculated at a rotational frequency of $\hbar\omega = 0.0$ MeV (left panel) and at $\hbar\omega = 0.94$ MeV (right panel) in ^{74}Kr for the ground-state band. Note the drastic change in deformation from $\beta_2 = 0.36$ at $\hbar\omega = 0.0$ to $\beta_2 = 0.28$ at $\hbar\omega = 0.94$.
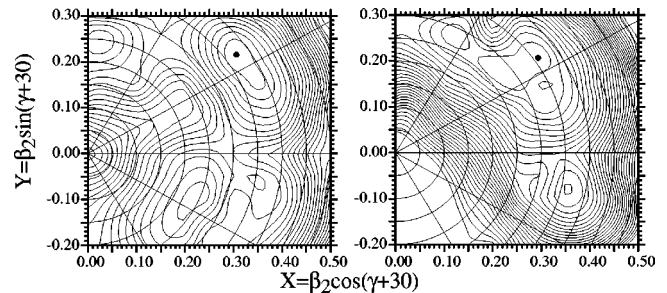

FIG. 6. The total Routhian surface for the negative parity side band calculated at low (left panel) and at high rotational frequency (right panel) in ^{74}Kr. No sensible change in deformation is observed from $\hbar\omega = 0.0$ (left panel) to $\hbar\omega = 0.94$ (right panel).

2QP excitation from the [312]3/2 into the [431]3/2 Nilsson orbit, there is a slight increase of the intrinsic quadrupole moment of this configuration. Nevertheless, the measured and calculated shape is somewhat smaller, again indicating the gain in rotational energy at reduced deformation. Since further proton alignment is blocked, we are dealing only with the effect arising from the neutrons. In the spin range of $I = 3–21\hbar$, we calculate a slight reduction from $Q_t = 3.3$ e b to $Q_t = 3.0$ e b. This effect is too small to be verified by the present measurement. Again the pronounced difference from the S-band is related to the effect that for neutrons, which are

higher in the shell, $dI/d\beta$ is smaller than for protons and hence the driving force is weaker.

In conclusion, we have extracted lifetime values of a large set of states in ^{74}Kr. The deduced quadrupole moments show strong configuration dependent shape effects. The deformation of the excited 2QP configuration of negative parity appears rather stable with spin, whereas the ground band experiences quite a dramatic shape change after the S-band crossing. The shape change is explained by the competition between the contribution of single particle and collective degrees of freedom to the rotational energy, favoring smaller deformation for the S-band.

[1] W. Nazarewicz *et al.*, Nucl. Phys. **A435**, 397 (1985).

[2] I. Ragnarsson, S. G. Nilsson, and R. K. Sheline, Phys. Rep. **45**, 1 (1978).

[3] P. Bonche *et al.*, Nucl. Phys. **A443**, 39 (1985).

[4] P.-H. Heenen, P. Bonche, J. Dobaczewski, and H. Flocard, Nucl. Phys. **A561**, 367 (1993).

[5] A. Petrovici *et al.*, Nucl. Phys. **A605**, 290 (1996).

[6] S. L. Tabor *et al.*, Phys. Rev. C **41**, 2658 (1990).

[7] J. Heese *et al.*, Phys. Rev. C **43**, R921 (1991).

[8] C. Chandler *et al.*, Phys. Rev. C **56**, R2924 (1997).

[9] D. Bazzacco, International Conference on Nuclear Structure at High Angular Momentum, Ottawa, 1992, AECL 10613, Vol. 2, p. 376.

[10] J. C. Wells and N. Johnson, Report No. ORNL-6689 (1991), p. 44.

[11] J. Lindhard, M. Scharff, and H. E. Schiott, Mat. Fys. Medd. K. Dan. Vidensk. Selsk. **33**, No. 14, 1 (1963).

[12] F. James and M. Roos, Comput. Phys. Commun. **10**, 343 (1975).

[13] S. H. Sie, D. Ward, J. S. Geiger, R. L. Grahan, and H. R. Andrews, Nucl. Phys. **A291**, 443 (1977).

[14] L. C. Northcliffe and R. F. Schilling, Nucl. Data, Sect. A **7**, 233 (1970).

[15] D. Rudolph *et al.*, Phys. Rev. C **56**, 98 (1997).

[16] P. Federman and S. Pittel, Phys. Lett. **69B**, 385 (1977).

[17] W. Satuła, R. Wyss, and P. Magierski, Nucl. Phys. **A578**, 45 (1994).

[18] W. Satuła and R. Wyss, Phys. Rev. C **50**, 2888 (1994).

[19] W. Satuła and R. Wyss, Phys. Scr. **T56**, 159 (1995).

[20] J. D. Garrett *et al.*, in *Proceedings of the Conference on Contemporary Topics in Nuclear Structure Physics*, Cocoyoc, Mexico, edited by R. Casten, A. Frank, M. Moshinsky, and S. Pittel (World Scientific, Singapore, 1988), p. 699.

[21] H. Xie *et al.*, Nucl. Phys. **A599**, 560 (1996).

[22] W. Satuła, R. Wyss, and F. Dönau, Nucl. Phys. **A565**, 573 (1993).

[23] B. Cederwall *et al.*, Phys. Rev. Lett. **72**, 3150 (1994).